Thrust and Efficiency of the K-III MPD Thruster

Takao Yoshikawa* and Yoichi Kagaya†
Osaka University, Osaka, Japan

and

Kyoichi Kuriki‡
Institute of Space and Astronautical Science, Tokyo, Japan

A quasisteady multimegawatt magnetoplasmadynamic (MPD) thruster, Komaba III, has been investigated to obtain fundamental thruster characteristics. The data presented in this paper are obtained with various propellants (Ar, NH_3, He, and H_2) for discharge currents ranging between 3 and 25 kA. Three different modes, diffuse, spot, and gross erosion, are found to exist in an MPD arc and a qualitative explanation of their nature is presented. Cathode and anode erosion are discussed and a preferred operating current for the thruster is identified at a current just below a limiting value, defined by electrode erosion. Thrust efficiencies are found to increase with specific impulse, reaching values of 32% at 4500 s for hydrogen propellant and 21% at 2500 s for ammonia.

Nomenclature

g = standard acceleration of gravity
I_{sp} = specific impulse
J = discharge current
J_c = critical current
J^* = limiting current
M = mass of atom or molecule
$\dot{m}$ = propellant mass flow rate
r_a = anode radius
r_c = cathode radius
T = measured thrust (electromagnetic + electrothermal thrust)
T_m = electromagnetic thrust
T_p = thrust-power ratio
U = exhaust velocity
U_c = critical ionization velocity
V = discharge voltage
α = self-field electromagnetic thrust coefficient
ϵ_d = dissociation energy
ϵ_i = ionization energy
η = thrust efficiency
μ = permeability of free space

Introduction

SINCE the magnetoplasmadynamic (MPD) thruster is a simple, efficient, and reliable device suitable as a future thruster in space, it is probably near space application. However a few questions remain to be answered before the projected space-qualified MPD thruster is translated into reality. These include defining the optimum thruster geometry, propellant, and lifetime. Of particular interest in the present experiment is the influence of various propellants on thrust, discharge voltage, thrust efficiency, and electrode erosion. Argon, ammonia, helium, and hydrogen are discussed as propellants.

It has been reported[1-3] that an upper "critical" limit of the discharge current exists for a given propellant flow rate, above which the operation of the thruster becomes increasingly unacceptable due to significant electrode erosion. Electrode erosion plays a key role in an assessment of the MPD thruster performance and is basically connected to the arc mechanism. Because of the extreme environment in an MPD arc, it is difficult to investigate electrode erosion mechanisms experimentally, but the discharge voltage and its fluctuation can serve as a key for the understanding of the MPD arc discharge.

For the present studies, a new quasisteady MPD thruster, Komaba III, was prepared and installed in the plasma wind tunnel at Osaka University. The operating propellant flow range for the present experiment varied from 0.6 to 3.0 g/s for argon propellant, 0.2 to 2.4 g/s for ammonia, 0.5 to 1.4 g/s for helium, and 0.2 to 1.4 g/s for hydrogen with discharge currents from 3 to 25 kA. This paper reports preliminary results of thruster performance testing in the form of measured voltage-current and thrust efficiency-specific impulse relations for the K-III MPD thruster, operating on various propellants. The cathode weights measured before and after two hundred pulse operations at a current of 10 kA were used to determine the cathode erosion rates.

Experimental Apparatus

The geometry of the K-III MPD thruster has been described in detail previously.[4,5] The thruster, as shown in Fig. 1, has a 32-mm long and 9.5-mm diameter thoriated tungsten cathode; the anode is an annular copper cylinder of 36 mm i.d. The outer surface of the thruster is insulated with fiber reinforced plastic (FRP) and ceramics. The discharge chamber is provided with propellant injection ports and sleeve electrodes (CF and AF), that operate at floating potential and are useful in relaxing current concentrations near the anode and cathode bases. In the discharge chamber are two annular slits from which the propellant is injected. The anode slit is between the anode inner surface and the floating electrode (AF); the cathode slit is between the cathode outer surface and the floating electrode (CF). The propellant injection system uses a fast acting valve (FAV) to provide a short gas pulse. The propellant, which is stored in an annular gas reservoir before each run, is introduced into the anode and cathode slits through eight choked orifices via flexible rubber tubes and gas ports. The FAV is driven by a 150 μF capacitor, charged to 1.4 kV and triggered by a silicon-controlled rectifier at the start of each run. The propellant gas density near the exit of the MPD thruster, measured with a fast ionization gage,[6] was

Presented as Paper 82-1887 at the AIAA/JSASS/DGLR 16th International Electric Propulsion Conference, New Orleans, La., Nov. 17-19, 1982; received Dec. 10, 1982; revision received Oct. 10, 1983. This paper is declared a work of the U.S. Government and therefore is in the public domain.

*Associate Professor, Department of Mechanical Engineering, Faculty of Engineering Science. Member AIAA.

†Engineer, Department of Mechanical Engineering, Faculty of Engineering Science.

‡Professor. Member AIAA.

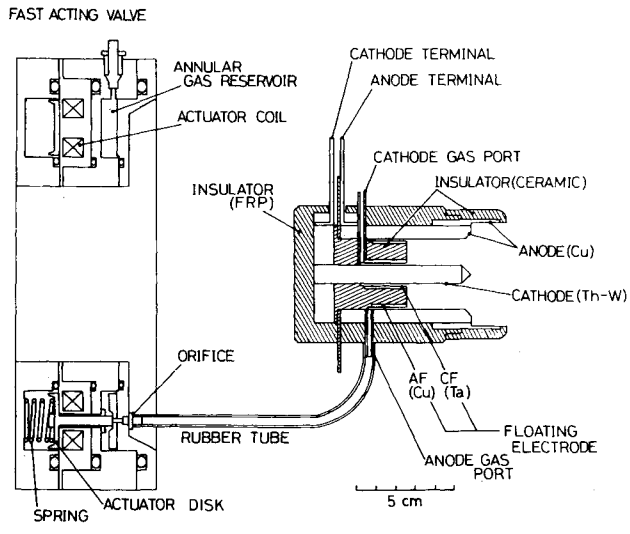

Fig. 1 Schematic diagram of new K-III MPD arcjet and fast acting valve.

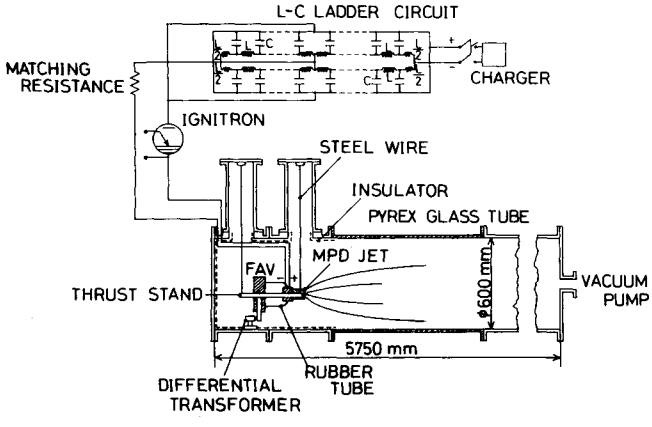

Fig. 2 Thrust stand installation in vacuum tank and pulse forming network.

found to rise in 0.5 to 1.0 ms and stay at that value for about 6 ms. The mass flow rate was controlled by the orifice diameter and reservoir pressure of the FAV.

The MPD thruster and FAV are mounted on a thrust stand suspended from the ceiling of a vacuum tank with four steel wires, as shown in Fig. 2. The thruster package on the thrust stand weighs approximately 8 kg and the system has a natural frequency of 1.2 Hz. The vacuum tank, 5.75 m in length and 0.6 m in diameter, is evacuated to less than 2×10^{-5} Torr before the experiment. The tank pressure remained below 10^{-4} Torr after a pulse of argon propellant was injected at a rate of 3 g/s.

The MPD thruster is driven by a pulse forming network (PFN), which is a 40-station, L-C ladder network capable of storing 62 kJ at 8 kV. For these tests, the PFN supplied single nonreversing current pulses of up to 25 kA for 0.6 ms. Switching is provided by an ignitron, triggered at 2.2-3.4 ms after the FAV is triggered, to allow sufficient time for the establishment of steady flow in the discharge chamber.

To study the characteristics of the MPD thruster, four quantities were measured: propellant mass flow rate ($\dot{m}$), thrust (T), discharge voltage (V), and discharge current (J). The quasisteady mass flow rate was calibrated using the pressure rise in the vacuum tank after the pulse propellant injection with the pumps shut off. The measured mass flow rates were 5 to 10% less than the values evaluated theoretically for choking conditions at the FAV orifice throat. However, the

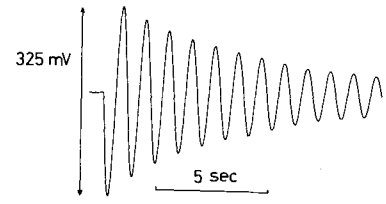

Fig. 3 Output signal of differential transformer. The signal indicates the vibration of a single-degree-of-freedom system with a period of about 1.2 Hz.

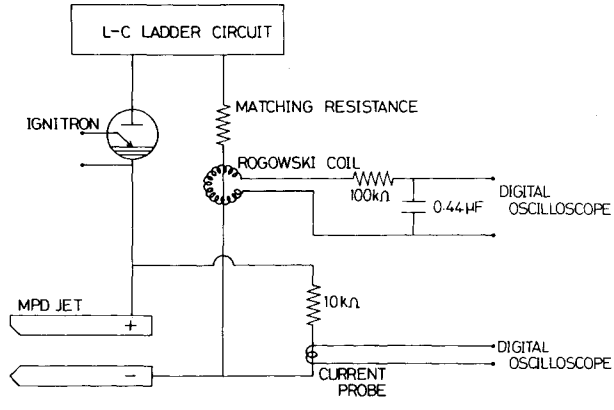

Fig. 4 Discharge current and voltage measurements.

mass flow rate in the present paper was determined from the theoretical value, because it is too troublesome to calibrate accurately for each reservoir pressure and propellant.

The thrust measurement is carried out by a pendulum method. The position of the thrust stand is detected by a linear differential transformer. The typical output signal from the differential transformer is shown in Fig. 3 which indicates the vibration of a single-degree-of-freedom system with a viscous damper. Current connectors, propellant feed, and instrumentation leads at the thrust stand act as the viscous dampers. The thrust was obtained from the displacement calibrated by applying an impulse of known magnitude using a small steel ball in an atmospheric pressure environment. Moreover the thrust due to the arc discharge alone is obtained by subtracting the thrust due to cold gas flow from the measured thrust which is determined using data such as that of Fig. 3.

The discharge current is measured outside the vacuum tank with a calibrated Rogowski coil, as shown in Fig. 4. Voltage measurements are made with a current probe (Iwatsu CP-502), which monitors the small current bled through a known resistor (10 kΩ) between the electrodes. The thrust, discharge voltage, and current data measured during the quasisteady current pulse of 0.6 ms are recorded and stored by two digital oscilloscopes. The discharge voltage measurement system has the maximum frequency response of about 1 MHz.

Experimental Results

It has been reported in Ref. 4 that the propellant injection from the anode slit is efficient in reducing the discharge voltage and enhancing the thrust efficiency for smaller total mass flow rates ($\dot{m} < 0.6$ g/s) of argon propellant. However the characteristics of the MPD thruster were found to be largely uninfluenced by the method of propellant injection, possibly because of greater propellant density in the discharge chamber at greater flow rates. The following data are obtained with 50% propellant supplied from the anode slit and 50% from the cathode slit.

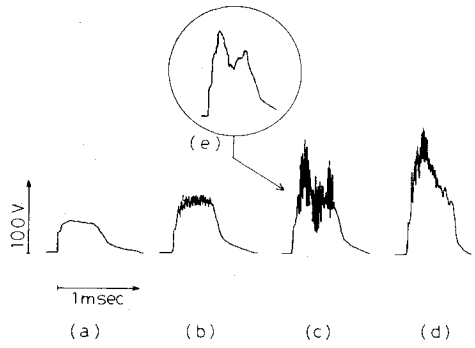

Fig. 5 Typical waveforms of discharge voltage, propellant: Argon, $\dot{m}$: 2.42 g/s, a) $J = 8.0$ kA, b) $J = 12.5$ kA, c) $J = 16.5$ kA, d) $J = 17.2$ kA, e) voltage waveform obtained using a low-pass filter of 20 kHz.

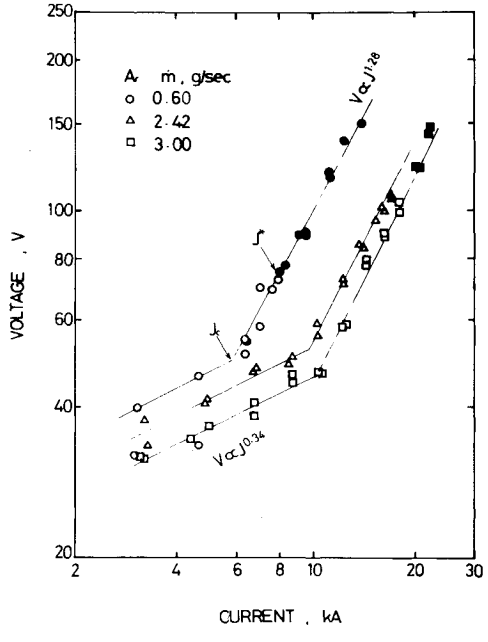

Fig. 6 Voltage-current characteristics for argon propellant. Solid symbols represent the operation at the current beyond J^*.

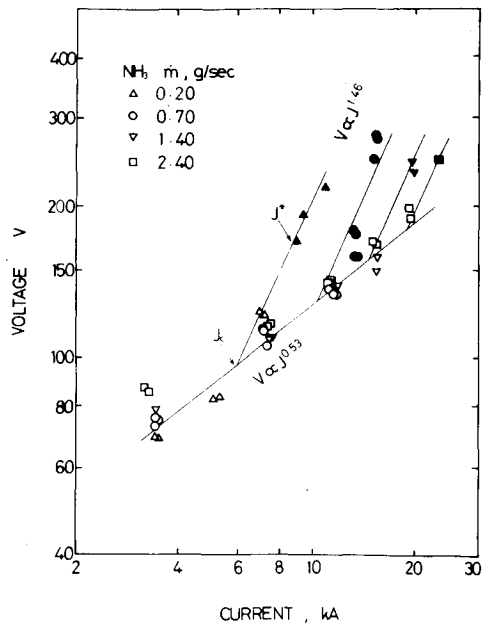

Fig. 7 Voltage-current characteristics for ammonia propellant. Solid symbols are the same as in Fig. 6.

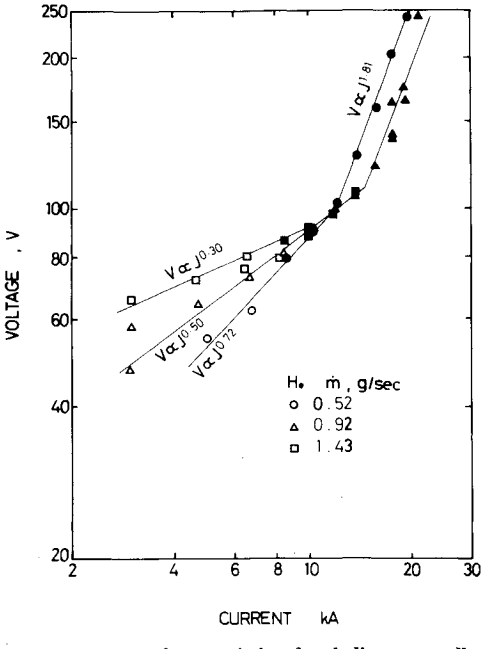

Fig. 8 Voltage-current characteristics for helium propellant. Solid symbols are the same as in Fig. 6.

Voltage-Current Characteristics

Typical waveforms of the discharge voltage for a given mass flow rate at various discharge currents are shown in Fig. 5. Figure 5e shows the voltage signal obtained using a low-pass (20 kHz) filter to measure a reasonable mean value of Fig. 5c. As the current is raised in the MPD arcjet, a transition occurs between low- and high-current modes of operation. Below a threshold current, the voltage waveform is quiescent, as shown in Fig. 5a; beyond the threshold current, the voltage gradually becomes unstable and fluctuates with random frequencies of at least 1 MHz. If the current is raised further, a second transition occurs, characterized by a quieting of the voltage waveform (Fig. 5d). At the second transition, gross erosion of the anode was observed. The voltage waveforms for H_2 and He were similar to those shown in Fig. 5 for argon, though they were relatively noisy, even at lower currents. The "limiting current, J^*," is defined here as that current for which the voltage waveform changes from a rectangular form to another one; that is, the mean squared deviation of the discharge voltage obtained using the low-pass filter is approximately 10% of the average voltage over the total current pulse of 0.6 ms. For example, the limiting current in Fig. 5 is between 12.5 kA (Fig. 5b) and 16.5 kA (Fig. 5c). It is considered that the operation of the MPD thruster is unacceptable beyond the critical current due to gross anode erosion. In the following figures, solid symbols indicate the operation of the MPD thruster at a current beyond the limiting value.

The voltage-current characteristics for the propellant of Ar, NH_3, He, and H_2 are shown in Figs. 6-9 for a range of mass flow rate. The results obtained depended on the atomic weight of the propellant. In the cases of Ar and NH_3, which are presented in Figs. 6 and 7, the slopes of the logarithmically plotted voltage-current curves are found to be relatively constant up to a particular current and then to jump abruptly to a larger constant at the current defined as the "critical current." The measured critical current (J_c) and limiting current (J^*) are summarized in Table 1. The theoretical model used to compute critical currents will be described later when the table is being discussed.

The discharge voltage (V) was found to increase with the discharge current (J). It has been observed[5,7] that V is nearly

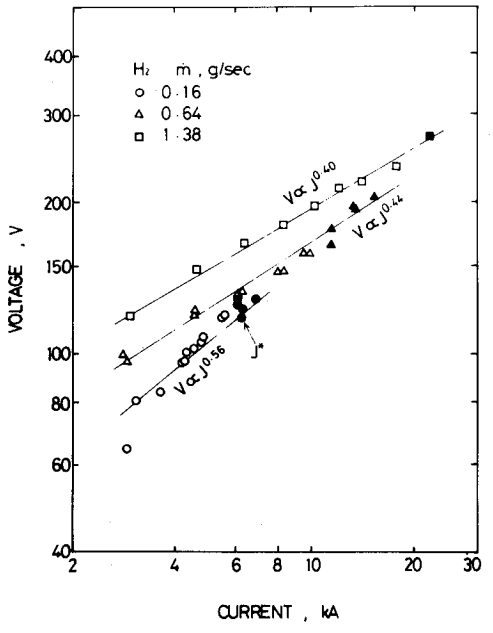

Fig. 9 Voltage-current characteristics for hydrogen propellant. Solid symbols are the same as in Fig. 6.

Table 1 Measured critical current, limiting current, and $J_c^2/\dot{m}$

Propellant	$\dot{m}$, g/s	J_c, kA	J^*, kA	$J_c^2/\dot{m}$, $(\text{kA})^2/\text{gs}^{-1}$	
Argon	0.60	5.8 (5.0)+	7.9	56	
	2.42	9.6 (10.1)	15.4	38	(42)[a]
	3.00	10.5 (11.2)	20.2	36	
Ammonia	0.20	5.9 (5.0)	7.2	174	
	0.70	10.2 (9.3)	11.0	148	(125)
	1.40	14.6 (13.2)	15.2	152	
	2.40	18.8 (17.3)	21.2	147	
Helium	0.52	(9.3)	6.8		
	0.92	(12.3)	8.4		(165)
	1.43	(15.4)	10.5		
Hydrogen	0.16	(6.5)	6.0		
	0.64	(13.1)	11.3		(266)
	1.38	(19.2)	18.7		

[a]( ) indicates a theoretical value. The model used to compute critical currents will be given later.

proportional to J at small J and to the third power of J at large J for smaller mass flow rates of argon. However the present results showed that V is proportional to $J^{0.34\text{-}0.71}$ below the critical current and to $J^{1.3\text{-}1.8}$ above the critical current. As the mass flow rate was increased, the following three situations describing the voltage rise or fall were observed: 1) Ar (heavy gas)—V becomes lower with increasing $\dot{m}$; 2) NH_3 (molecular gas)—V is insensitive to $\dot{m}$; 3) H_2 and He (light gases)—V becomes higher with increasing $\dot{m}$. These differences can be interpreted as follows: The input power, which is proportional to V at constant J, is spent mainly in heating and accelerating the propellant gas. The heating power, including that required for dissociation and ionization, is proportional to $\dot{m}$; the power required for acceleration is inversely proportional to $\dot{m}$, since the electromagnetic thrust is considered to be dominant.[5] For lighter gases, the power dissipated in dissociation and ionization is greater than that dissipated in the production of electromagnetic thrust at small J because of a larger number of gas particles for a given mass flow rate. Thus, the discharge voltage for H_2 and He increases with increasing $\dot{m}$.

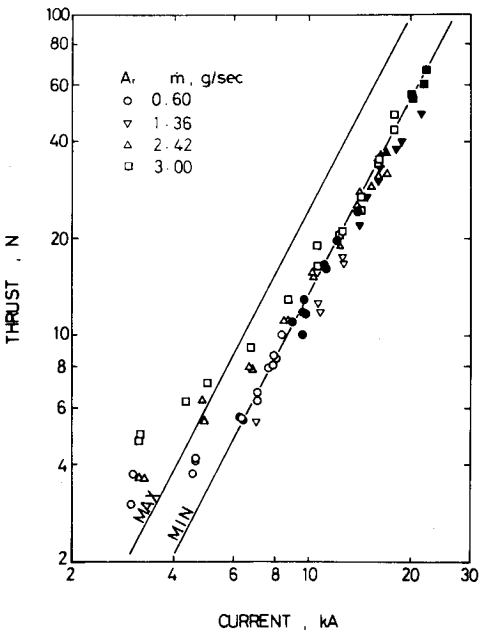

Fig. 10 Thrust-current characteristics for argon. Solid symbols indicate the operation at the current beyond J^*. Solid lines represent theoretical predictions. MAX: $T_m = 10^{-7}\,[\ell n(r_a/r_c) + \frac{3}{4}]J^2$ with $r_a/r_c = 26/4.75$; MIN: $T_m = 10^{-7}\,[\ell n(r_a/r_c)]J^2$ with $r_a/r_c = 18/4.75$.

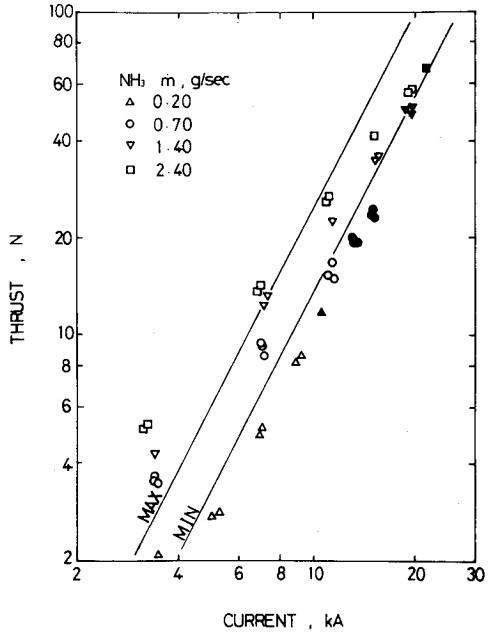

Fig. 11 Thrust-current characteristics for ammonia. Solid symbols, MAX and MIN lines are the same as in Fig. 10.

Thrust-Current Characteristics

The measured thrust is plotted as a function of the discharge current in Figs. 10-13 for Ar, NH_3, He, and H_2, respectively. The solid lines in these figures represent the theoretical prediction of electromagnetic thrust given by[8]:

$$\text{MAX: } T_m = (\mu/4\pi)J^2[\ell n(r_a/r_c) + 3/4] \quad (1)$$

$$\text{MIN: } T_m = (\mu/4\pi)J^2\ell n(r_a/r_c) \quad (2)$$

At high-current conditions, the thrust for Ar, NH_3, and He approaches the predicted MIN line; that for H_2 approaches the MAX line. These figures show that the thrust varies as the

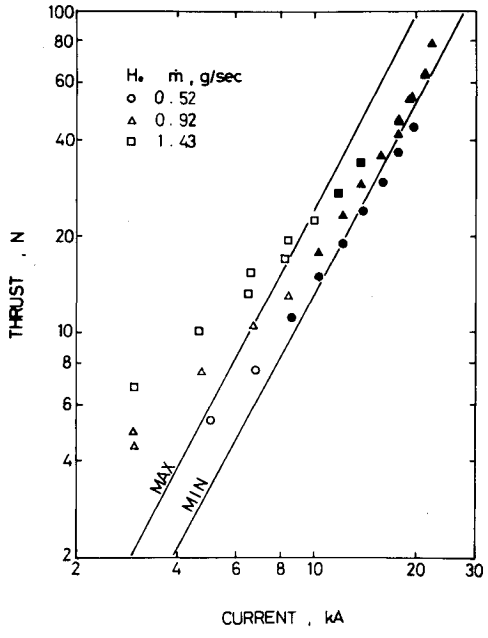

Fig. 12 Thrust-current characteristics for helium. Solid symbols, MAX and MIN lines are the same as in Fig. 10.

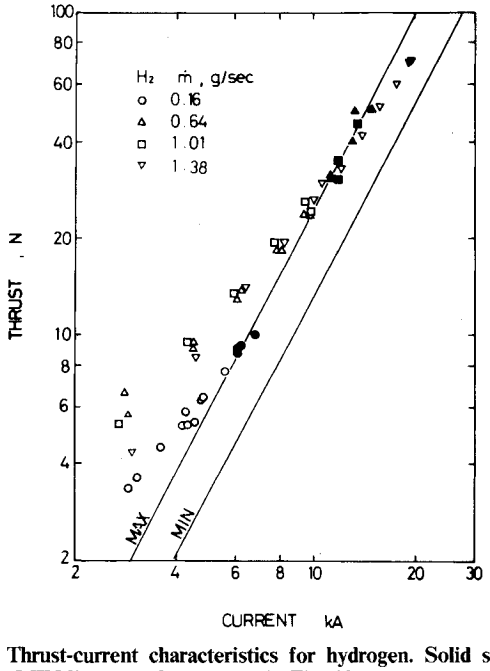

Fig. 13 Thrust-current characteristics for hydrogen. Solid symbols, MAX and MIN lines are the same as in Fig. 10.

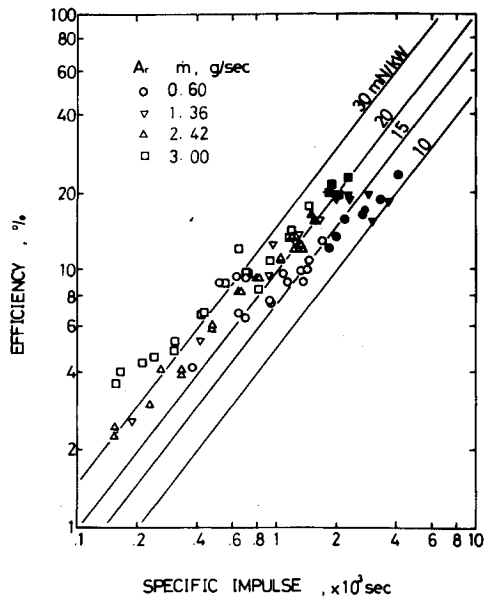

Fig. 14 Thrust efficiency vs specific impulse for argon. Solid lines represent thrust power ratio of 10, 15, 20, and 30 mN/kW, respectively.

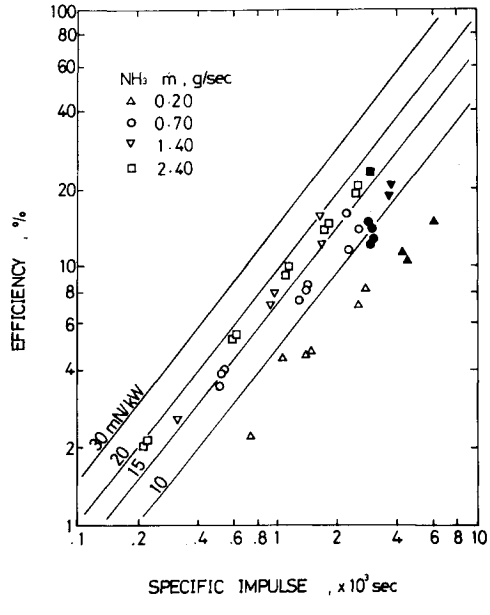

Fig. 15 Thrust efficiency vs specific impulse for ammonia. Solid lines are the same as in Fig. 14.

second power of the current and is insensitive to $\dot{m}$, as Eqs. (1) and (2) suggest. The electrothermal component of thrust, which should be linearly proportional to J, is observed only at low-current conditions. In the case of H_2 and He, the greater contribution of the electrothermal component is particularly apparent at small J. It is worthy of notice that the thrust-current characteristics for NH_3 in Fig. 11 are similar to those for H_2 at large $\dot{m}$ and to those for Ar at small $\dot{m}$.

Thrust Efficiency

The measured discharge current, voltage, and thrust are used to predict quasisteady values for specific impulse and thrust efficiency through the relations

$$I_{sp} = T/\dot{m}g = U/g \tag{3}$$

$$\eta = T^2/2\dot{m}VJ \tag{4}$$

$$T_p = T/VJ \tag{5}$$

where T_p is the thrust-power ratio defined as the ratio of the thrust to the discharge power. The thrust efficiency is shown as a function of I_{sp} in Figs. 14-17 for Ar, NH_3, He, and H_2, respectively. In these figures, solid lines represent thrust-power ratios of 10, 15, 20, and 30 mN/kW. From these data, the efficiency is found to increase with specific impulse, hence with discharge current. The maximum efficiency was obtained at the previously defined limiting current. The efficiency at the current near the limiting value for the propellant used are summarized in Table 2. For specific impulses greater than 1000 s, which are of practical interest for high-power MPD thrusters, the efficiency for H_2 is higher than that for Ar.

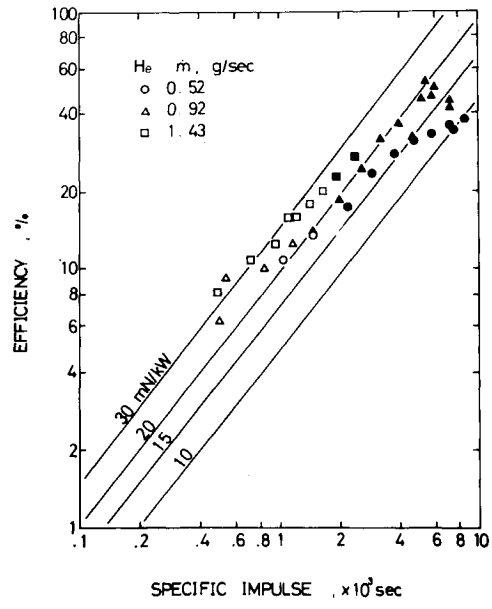

Fig. 16 Thrust efficiency vs specific impulse for helium. Solid lines are the same as in Fig. 14.

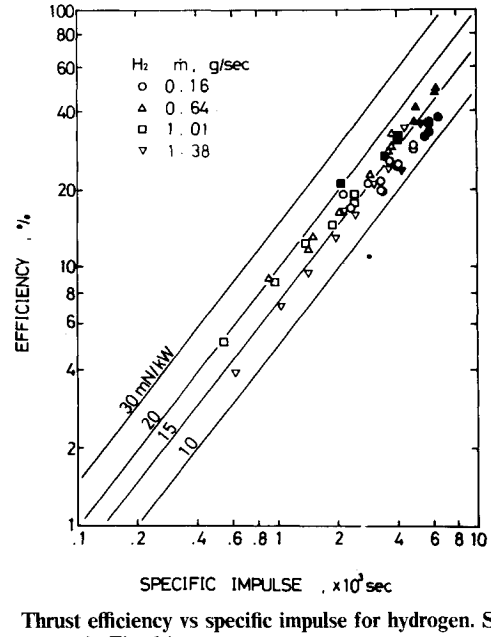

Fig. 17 Thrust efficiency vs specific impulse for hydrogen. Solid lines are the same as in Fig. 14.

Table 2 Maximum thrust efficiencies for several propellant species

Propellant	$\dot{m}$, g/s	J, kA	η, %	I_{sp}, s
Argon	3.00	18.0	17	1550
Ammonia	2.40	18.9	21	2450
Helium	1.43	10.5	20	1900
Hydrogen	1.38	17.7	32	4500

Table 3 Cathode erosion with several propellant species

Propellant	$\dot{m}$, g/s	J, kA	Cathode loss, μg/C
Argon	3.00	10.0	5.1
Ammonia	2.40	10.0	8.7
Helium	1.43	9.8	12.5
Hydrogen	1.38	10.0	15.1

Electrode Erosion

A series of experiments was undertaken in which the amount of material eroded from the thoriated tungsten cathode was measured at the current of about 10 kA. The cathode was weighted with a precision balance after two hundred pulses. Cathode loss is defined as the mass loss divided by the integral of discharge current over the discharge duration of 0.6 ms and is expressed in $\mu g/C$, as shown in Table 3. From Table 3, it should be noted that the cathode loss depends strongly on the gas species for a given current. The cathode loss is greater for lighter gases than it is for the heavier ones. Cathode erosion occurred mainly at the cathode tip and its surface had many craters smaller than 0.1 mm in diameter.

From these and results obtained at lower current levels, which are not shown here, it is suggested that many spots develop on the cathode surface of the MPD arcjet over the region from which the discharge electrons are drawn; cathode vapor and electrons are ejected from the region of cathode spots to sustain the MPD arc; and the magnitude of cathode loss depends on the extent of current concentration on the cathode tip.

Anode erosion, though not measured quantitatively, was not observed below the critical current. The anode surface was smoothly and uniformly burned by the MPD arc and had no craters on its surface. As the discharge current was raised further, the anode surface became somewhat rough after more than 100 shots. Beyond the limiting current, J^*, the gross anode erosion was observed, especially at the edge of the anode front surface. The cathode jet may be strongly constricted at high-power operations by a self-magnetic field and the discharge current is extended far downstream. This causes the current to be concentrated at the edge of the anode front surface. This effect is more prominent for H_2 than it is for Ar.

Discussion

As the discharge current is increased, three discharge modes in the MPD arc similar to a vacuum arc[9-14] were suggested by the results of the V-J characteristics and the electrode erosion tests.

Diffuse Mode ($J < J_c$)

Below the critical current, the MPD arc shows a diffuse appearance and covers the annular anode uniformly. The voltage waveform was quiescent as shown in Fig. 5a. Since the anode loss was not observed at all, the anode surface temperature is estimated to remain below the melting point of copper, similar to vacuum arc results.[13,14] The anode does not affect the discharge significantly and functions only as a condensing surface for electrons and cathode vapor.

Spot Mode ($J_c \leqq J < J^*$)

If the critical current is reached, the MPD arc changes to a new, destructive mode. Many small anode spots form nonuniformly on the anode surface. The random motion of these spots and fluctuations of the anode fall voltage[4] may cause the high-frequency fluctuations of the discharge voltage as shown in Fig. 5b. Anode spot temperatures exceeding the melting point of copper are suggested from the results of the electrode erosion tests and theoretical estimation in Refs. 13 and 14. Further increases in current are accompanied by a highly unstable discharge voltage. The mean voltage increases with current as shown in Figs. 6-9. The current at which the sudden rise of the slope in the V-J curve on a log-log plot develops was termed the "critical current J_c." The critical current was not generally consistent with the limiting current J^* which was defined from the waveforms of the mean discharge voltage (Fig. 5). It has been reported[4] that the discharge voltage drops at the point where anode spots begin to be observed. Such phenomena could not be confirmed in the present experiments due to nonuniformity of current distributions.

Several authors[15-18] have discovered that when the relative velocity between a plasma and a neutral gas in a magnetic field reaches or exceeds a critical value, the gas is efficiently ionized. This velocity is determined by the condition that the kinetic energy is equal to the ionization energy of the gas. This critical ionization velocity was first pointed out by Alfvén.[15] This rough theory, applied to the K-III MPD geometry, is presented as follows:

At the critical ionization velocity where

$$MU_c^2/2 = \epsilon_d + \epsilon_i \tag{6}$$

the electromagnetic thrust is described by

$$T_m = \alpha J_c^2 = \dot{m} U_c \tag{7}$$

where α is constant, which is determined by the configuration of discharge current given by Eqs. (1) and (2). An expression for the parameter $J_c^2/\dot{m}$ is now derived by a combination of Eqs. (6) and (7):

$$J_c^2/\dot{m} = U_c/\alpha = \left[2(\epsilon_d + \epsilon_i)/M\right]^{\frac{1}{2}}/\alpha \tag{8}$$

A relation similar to Eq. (8) was recently proposed by Baksht et al.[19] They pointed out that an anode instability is brought about by a process of ion starvation close to the anode.

In addition to the measured currents J_c and J^*, the values of J_c and $J_c^2/\dot{m}$ obtained from Eqs. (7) and (8) are summarized in Table 1. For argon and ammonia propellants, the critical current in the present experiment seems to correspond to the critical ionization speed or starvation condition near the anode. The fluctuation level of the voltage is related strongly to the propellant. The voltage waveform for argon was considerably quieter and its mean value still rectangular above the critical current; gross anode erosion did not occur. Otherwise, the limiting current for ammonia was nearly equal to the critical current. The observations above were not found for the cases of helium and hydrogen propellants.

Gross Erosion Arc Mode ($J \geqq J^*$)

If the discharge current is extended beyond J^*, the discharge voltage, which is highly unstable, continues to increase until the onset of gross anode erosion. Once gross anode erosion occurs, the mean level of the voltage may fall even though the current is increasing. The high-frequency fluctuations then disappear and the voltage waveform becomes quieter. In this mode, it was quite hard to obtain reproducible voltage waveforms. After a shot, a few longitudinal streaks 5-10 mm in length and 0.1-0.5 mm in width were observed on the anode surface near the exit. This suggests that the anode spots are being blown downstream by the electromagnetic body force.

Summary and Conclusions

In the experiment of a K-III MPD thruster, the following results were obtained:

1) As the discharge current was increased, the three different modes of operation, diffuse, spot, and gross erosion, were observed. The current at the first transition, J_c, was determined from the sudden slope rise in the V-J curve on the log-log plot and agreed with the value calculated from the critical ionization speed or anode starvation condition for Ar and NH_3 propellants. The limiting current, J^*, at which gross erosion occurs, was greater than the critical current when argon propellant was being used, and was nearly equal to the critical current in the case of ammonia. The limiting currents obtained using helium and hydrogen were smaller than the calculated critical current.

2) In the V-J characteristics, the discharge voltage was proportional to $J^{0.34\text{-}0.71}$ below J_c and to $J^{1.3\text{-}1.8}$ above J_c. As the mass flow rate was increased, the following three situations were observed: a) Ar: V becomes lower with increasing $\dot{m}$, b) NH_3: V is insensitive to $\dot{m}$; c) H_2 and He: V becomes higher with increasing $\dot{m}$.

3) A preferred operating point for a given mass flow rate occurs at the current just below J^*. The hydrogen propellant was advantageous and the electrothermal acceleration had a significant contribution to the thrust.

4) The anode was not eroded in the diffuse mode, but was in the spot mode. Cathode erosion occurred over all ranges of the discharge current. The cathode loss depended strongly on the propellant species.

5) If some cathode erosion is allowed, the optimum propellant is hydrogen; if not, ammonia is preferred. The maximum efficiency for H_2 was 32% at a specific impulse of 4500 s; that for ammonia was 21% at 2500 s.

References

[1]Malliaris, A.C., John, R.R., Garrison, R.L., and Libby, D.R., "Quasi-Steady MPD Propulsion at High Power," Final Tech. Report AVSD-0146-71-RR, AVCO Corp.; NASA CR 111872, Feb. 1971.

[2]King, D.Q., Smith, W.W., John, R.R., and Clark, K.E., "Effect of Thrust Chamber Configuration on MPD Arcjet Performance," AIAA Paper 79-2051, 1979.

[3]Boyle, M.J., Clark, K.E., and Jahn, R.G., "Flowfield Characteristics and Performance Limitations of Quasi-Steady Magnetoplasmadynamic Accelerators," *AIAA Journal*, Vol. 14, July 1976, pp. 955-962.

[4]Kuriki, K., Onishi, M., and Morimoto, S., "Thrust Measurements of K III MPD Arcjet," *AIAA Journal*, Vol. 16, Oct. 1982, pp. 1414-1419.

[5]Kuriki, K. and Suzuki, H., "Transitional Behavior of MPD Arcjet Operation," *AIAA Journal*, Vol. 16, Oct. 1978, pp. 1062-1067.

[6]Inutake, M. and Kuriki, K., "Fast Ionization Gauge Studies of Quasisteady Gas Injection into Vacuum," *Review of Scientific Instruments*, Vol. 43, Nov. 1972, pp. 1670-1674.

[7]Clark, K.E. and Jahn, R.G., "Quasi-Steady Plasma Acceleration," *AIAA Journal*, Vol. 8, Feb. 1970, pp. 216-220.

[8]Jahn, R.G., *Physics of Electric Propulsion*, McGraw-Hill, New York, 1968, Chap. 8.

[9]Mitchell, G.R., "High Current Vacuum Arcs, Part 1-An Experimental Study," *Proceedings of the IEEE*, Vol. 117, Dec. 1970, pp. 2315-2326.

[10]Boxman, R.L., "Magnetic Constriction Effects in High-Current Arcs prior to the Release of Anode Vapor," *Journal of Applied Physics*, Vol. 48, June 1977, pp. 2338-2345.

[11]Schnöcker, D., "Improved Model for Anode Spot Formation in Vacuum Arcs," *IEEE Transactions on Plasma Science*, Vol. PS-7, Dec. 1979, pp. 209-216.

[12]Guile, A.E. and Jüttner, B., "Basic Erosion Process of Oxidized and Clean Metal Cathodes by Electric Arcs," *IEEE Transactions on Plasma Science*, Vol. PS-8, Sept. 1980, pp. 259-269.

[13]Cobine, J.D. and Burger, E.E., "Analysis of Electrode Phenomena in the High-Current Arc," *Journal of Applied Physics*, Vol. 26, July 1955, pp. 895-900.

[14]Miller, H.C., "Vacuum Arc Anode Phenomena," *IEEE Transactions on Plasma Science*, Vol. PS-5, Sept. 1977, pp. 181-196.

[15]Alfvén, H., "Collision between a Nonionized Gas and a Magnetized Plasma," *Review of Modern Physics*, Vol. 32, 1960, pp. 710-713.

[16]Fahleson, U.V., "Experiments with Plasma Moving through Neutral Gas," *Physics of Fluids*, Vol. 4, Jan. 1961, pp. 123-127.

[17]Patrick, R.M. and Schneiderman, A.M., "Performance Characteristics of a Magnetic Annular Arc," *AIAA Journal*, Vol. 4, Feb. 1966, pp. 283-290.

[18]Danielson, L., "Experiment on the Interaction between a Plasma and a Neutral Gas," *Physics of Fluids*, Vol. 13, Sept. 1970, pp. 2288-2294.

[19]Baksht, F.G., Moizhes, B.Y., and Rybakov, A.B., "Critical Regime of a Plasma Accelerator," *Soviet Physics Technical Physics*, Vol. 18, Dec. 1974, pp. 1613-1616.